On a computer-aided approach to the computation of Abelian integrals

Tomas Johnson
Department of Mathematics
Uppsala University
Box 480, 751 06 Uppsala, Sweden
johnson@math.uu.se

Warwick Tucker
Department of Mathematics
University of Bergen
Johannes Bruns gate 12, 5008 Bergen, Norway
warwick.tucker@math.uib.no

April 30, 2008

Abstract

An accurate method to compute enclosures of Abelian integrals is developed. It is applied to the study of bifurcations of limit cycles from cubic perturbations of elliptic Hamiltonians of degree four. We give examples of perturbations such that 2, 3, 3, and 4 limit cycles bifurcate from the truncated pendulum, the saddle loop, the interior of the cuspidal loop, and the interior of the figure eight loop, respectively. Some methods to find perturbations with a given number of limit cycles are illustrated in the examples.

1 Introduction

Nonlinear ordinary differential equations are one of the most common models used in any application of mathematical modelling. The most fundamental is perhaps the model of 1-dimension mechanical motion,

$$\ddot{x} = f(x, \dot{x}). \tag{1}$$

In this paper we study families of such equations

$$\ddot{x} + \epsilon f(x, \dot{x}) + g(x) = 0, \tag{2}$$

depending on a small constant ϵ.

A fundamental question about such systems is to determine the number and location of limit cycles bifurcating from the corresponding planar vector field

$$\left\{ \begin{array}{rcl} \dot{x} &=& -y \\ \dot{y} &=& \epsilon f(x, \dot{x}) + g(x) \end{array} \right. \tag{3}$$

as $\epsilon \to 0$.

In general, the question about the maximal number of limit cycles, and their location, of a polynomial planar vector field is the second part of Hilbert's 16th problem, which is unsolved even for polynomials of degree 2. For an overview of the progress that has been made to solve this problem we refer to [20]. Results for the degree 2 case, and a general introduction to the bifurcation theory of planar polynomial vector fields can be found in [31]. What is known, is that any given polynomial vector field can have only a finite number of limit cycles; this is proved in [11, 19].

A restricted version of Hilbert's 16th problem, known as the *weak*, or sometimes the *tangential*, or the *infinitesimal*, Hilbert's 16th problem, asks for the number of limit cycles that can bifurcate from a perturbation of a Hamiltonian system, see e.g. [3]. The weak Hilbert's 16th problem has been solved for the degree 2 case, see [2].

Special cases of Hamiltonian systems are the systems (2), which we study in this paper. If one assumes that $f(x, \dot{x}) = f(x)\dot{x}$, (2) is known as a Lienard equation. Such equations have been thoroughly studied, and the case where f, and g have degree 3 has been solved, see [6, 7, 8, 9]. We study general f of degree 3; the set-up of the problem is given in Section 2.

In this paper we present a rigorous, computer-aided approach to find limit cycles of planar polynomial vector fields. A different computer-aided approach was introduced by Malo in his PhD-thesis [22], (also described in [15, 16]) which is based on the concept of a rotated vector field, as introduced in [5]. Our approach is completely different: we develop a method to rigorously compute what is known as an Abelian integral. A brief introduction to Abelian integrals is included in Section 4. The concept of a computer-aided proof in analysis is based on techniques to rigorously enclose the result of a numerical computation. A basis for such a procedure is interval analysis, introduced by Moore in [23]. By calculating with sets rather than floating points, it is possible to obtain guaranteed results on a computer, enabling automated proofs for continuous problems.

The methods developed in this paper are neither restricted to any specific degree of the polynomial functions f, and g, nor to the case of systems of the form (3). It can be used to compute Abelian integrals of any polynomial perturbation from any family of compact level curves, ovals, of a polynomial Hamiltonian. In the examples given in this paper, however, we restrict to the case when f and g have degree 3.

2 Elliptic Hamiltonians of degree 4

We study the elliptic Hamiltonians of degree 4, given by

$$H(x, y) = \frac{y^2}{2} + a\frac{x^4}{4} + b\frac{x^3}{3} + c\frac{x^2}{2}, \tag{4}$$

corresponding to the differential system,

$$\left\{ \begin{array}{rcrcl} \dot{x} & = & -H_y & = & -y \\ \dot{y} & = & H_x & = & ax^3 + bx^2 + cx. \end{array} \right. \tag{5}$$

We are interested in limit cycles bifurcating from the periodic solutions of (5), corresponding to integral curves of (4). The closed level-curves of (4) are called *ovals*. In a series of papers [6, 7, 8, 9], Dumortier and Li study cubic perturbations corresponding to Lienard equations. That is,

$$\ddot{x} + \epsilon(\alpha + \beta x + \gamma x^2)\dot{x} + ax^3 + bx^2 + cx = 0, \tag{6}$$

or as a system,

$$\begin{cases} \dot{x} &= & -H_y \\ \dot{y} &= & H_x + \epsilon(\alpha + \beta x + \gamma x^2)y. \end{cases} \tag{7}$$

The purpose of this paper is to add a fourth term, $\delta\frac{y^3}{3}$, to the perturbation and to explore what kind of bifurcations we can prove to exist. We study the perturbed system,

$$\begin{cases} \dot{x} &= & -H_y \\ \dot{y} &= & H_x + \epsilon\left((\alpha + \beta x + \gamma x^2)y + \delta\frac{y^3}{3}\right). \end{cases} \tag{8}$$

The 1-form associated with this perturbation is

$$\omega = -\left((\alpha + \beta x + \gamma x^2)y + \delta\frac{y^3}{3}\right)\,dx. \tag{9}$$

For computational efficiency we primarily study its exterior derivative,

$$d\omega = \left((\alpha + \beta x + \gamma x^2) + \delta y^2\right)\,dx \wedge dy. \tag{10}$$

For the elliptic Hamiltonians of degree four with compact ovals, there are five different classes of phase portraits, see e.g [3]. They are, *the truncated pendulum, the saddle loop. the global centre, the cuspidal loop,* and *the figure-eight loop*, illustrated in Figure 1(i-v). In this paper we study cases (i),(ii), (iv), and (v). In the cases of the cuspidal loop and the figure eight loop, we restrict our study to the ovals inside the loops. The cases under study have the advantage that only compact intervals of values of the Hamiltonian have to be considered.

2.1 Known results

In [6, 7, 8, 9] Dumortier and Li prove that sharp bounds on the number of limit cycles bifurcating from (7) are $1, 2, 4, 4$, and 5, for the cases (i)-(v), respectively. They prove that the maximal number of limit cycles inside the loops in both cases (iv), and (v) is 2.

In [29] Petrov proves that the number of limit cycles bifurcating from (8) in case (v) is bounded by $n + [\frac{n-1}{2}] - 1$ in each of the two families of ovals inside the figure eight loop, for a polynomial perturbation of degree n. Liu studies the same case in [21], where he proves that the total number of limit cycles bifurcating from both families, is bounded by $2n-1$, and $2n+1$, for n even and odd, respectively. Liu also proves that the number of zeros outside the figure eight loop is bounded by $2n+1$, and $2n+3$, for n even, and odd, respectively. Petrov has also studied case (iii) – the global centre – in [30].

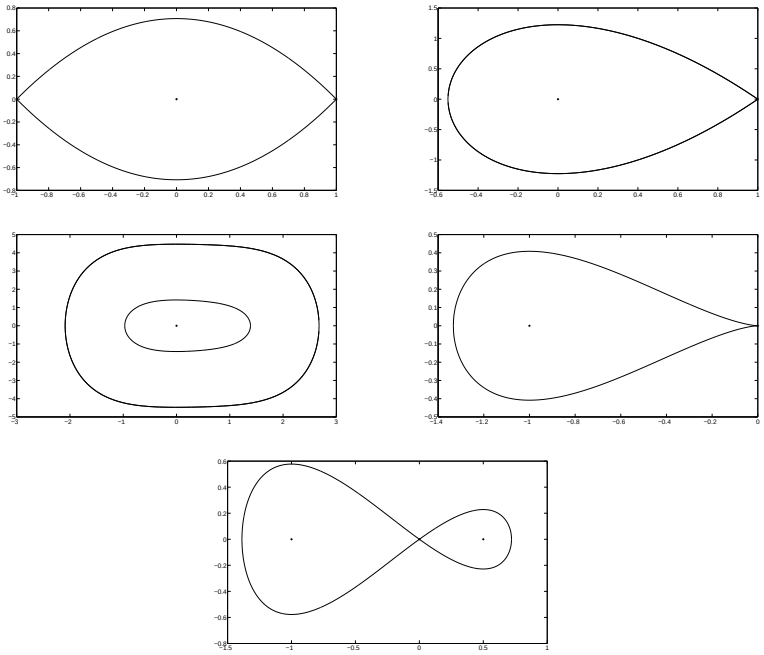

Figure 1: The elliptic Hamiltonians of degree 4.

3 Summation of the results

Theorem 3.1. *For the Elliptic Hamiltonian of degree 4, (4), there exists cubic perturbations with the following number of limit cycles:*
(i) The truncated pendulum: two limit cycles,
(ii) The saddle loop: three limit cycles,
(iii) The cuspidal loop: three interior limit cycles,
(iv) The figure eight loop: four interior limit cycles; two in each eye.

The examples mentioned in the theorem are illustrated in Figure 2. Note that we only prove existence of the limit cycles, their locations as drawn in the figure are only approximations.

4 Abelian integrals

A classical method to prove the existence of limit cycles bifurcating from a family of ovals of a Hamiltonian, $\Gamma_h \subset H^{-1}(h)$, depending continuously on h, is to study Abelian integrals, or, more generally, the Melnikov function, see e.g. [3, 14]. Some caution, however, must be taken regarding the correspondence between limit cycles and Abelian integrals, see e.g. [10]. Given a Hamiltonian system and a perturbation,

$$\begin{cases} \dot{x} &= -H_y + \epsilon f(x,y) \\ \dot{y} &= H_x + \epsilon g(x,y), \end{cases} \tag{11}$$

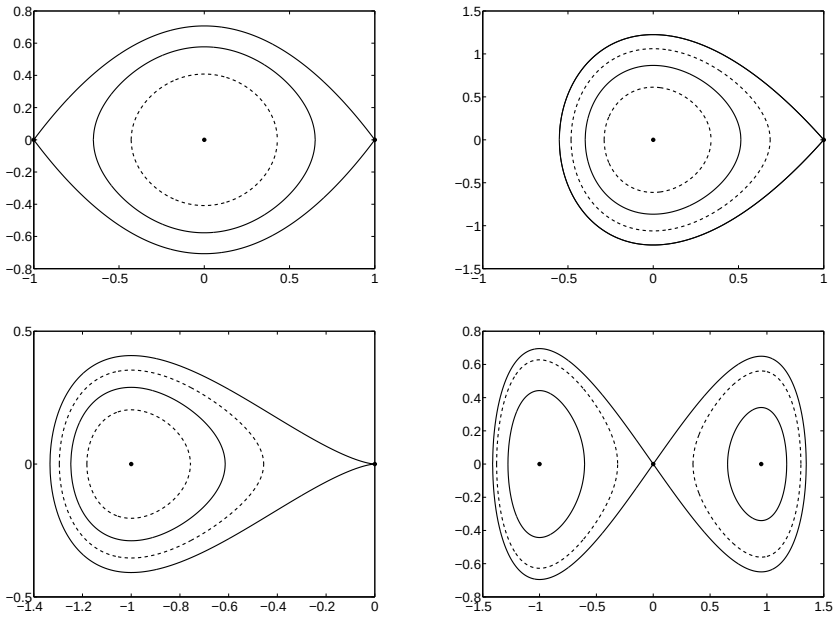

Figure 2: The limit cycles from Theorem 3.1. Unstable limit cycles are dashed.

the Abelian integral is defined as

$$I(h) = \int_{\Gamma_h} f(x,y)\,dy - g(x,y)\,dx. \tag{12}$$

In this paper all perturbations are polynomial. The most important property of Abelian integrals is described by the Poincaré-Pontryagin theorem. Let P be the return map defined on some section transversal to the ovals of H, parametrised by the values h of H, where h is taken from some bounded interval (a,b). We consider the displacement function $d(h) = P(h) - h$. The theorem by Poincaré-Pontryagin states that

$$d(h) = \epsilon(I(h) + \epsilon\phi(h,\epsilon)), \qquad \text{as} \quad \epsilon \to 0, \tag{13}$$

where $\phi(h,\epsilon)$ is analytic and uniformly bounded on a compact neighbourhood of $\epsilon = 0,\ h \in (a,b)$.

5 Computer-aided computation of Abelian integrals

5.1 Computer-aided proofs

To prove mathematical statements on a computer, we need an arithmetic which gives guaranteed results. Many computer-aided proofs, including the results in this paper, are based on interval analysis, e.g. [12, 17, 32]. Interval analysis

yields rigorous results for continuous problems, taking both discretisation and rounding errors into account. For a thorough introduction to interval analysis we refer to [1, 23, 24, 25, 27].

5.2 Outline of the approach

The main idea of this paper is to develop a very accurate, validated method to enclose the value of a general Abelian integral. Such a method enables us to sample values of $I(h)$. If we can find two ovals Γ_{h_1}, and Γ_{h_2}, such that

$$I(h_1)I(h_2) < 0, \tag{14}$$

then there exists $h^* \in (h_1, h_2)$, such that $I(h^*) = 0$.

Since P_ϵ, the return map of the perturbed vector field, is analytic and non-constant, it has isolated fixed points. Thus, we have proved the existence of (at least) one limit cycle bifurcating from Γ_{h^*}.

To construct perturbations such that the associated Abelian integral has a given number of zeros, the constants, α, β, γ, and δ in the form ω have to be chosen in a careful manner. The heuristic approach we have used to choose these constants is described in Section 6.

5.3 Computing the integrals

To compute the Abelian integral (12) of the form (9), we apply Stokes theorem to get

$$I(h) = \int_{D_h} dw, \tag{15}$$

where D_h denotes the interior of an oval Γ_h. The reason why we prefer to calculate surface integrals, rather than contour integrals, is that we cannot represent the ovals of H exactly. We can only find a cover of the ovals, and the area of this cover yields the uncertainty of our calculations, automatically handled by the interval arithmetic. If we had chosen to compute contour integrals, all of our computations would have been subjected to those errors, since we would always integrate over an unknown location. When calculating surface integrals, however, the effect of the uncertainty of the location of the ovals only contributes on a very small portion of the total area of D_h. Note that, inside D_h it is possible to integrate $d\omega$ exactly, that is, there are no truncation errors.

The actual computation of the integrals is performed in four steps; first we find a trapping region for the interesting family of ovals, second we adaptively split this region into three parts, one that covers the oval, one representing the inside and one representing the outside, third we change the coordinates on the boxes covering the oval in order to minimise the area of the cover, fourth we integrate $d\omega$ on the boxes representing the inside and the cover of the oval.

The first step is simple, since we only consider ovals that are situated inside a homo- or heteroclinic orbit. A short branch–and–bound algorithm quickly finds a box enclosing the homo- or heteroclinic orbit; this box is our initial domain used for the main part of the program.

In the second step – the adaptive splitting of the domain – we perform a series of tests to determine whether a box B intersects the oval, is inside it, or outside it. We start by evaluating the Hamiltonian on B using monotonicity

and central forms; since the Hamiltonians we study are sufficiently simple, we implement the derivatives symbolically. Three cases occur: if $H < h$, then B is inside the oval, and we label B as such. If $H > h$ then B is outside the oval and we ignore it. Finally, if $h \in H$, then we try to perform the change of variables as described below. If the change of variables procedure fails, and the size of B is greater than some stopping tolerance, `minsize`, then we split the box B into four parts and re–examine them separately. If the size of B is smaller than `minsize`, then it is labelled `fail`. If the change of variables procedure works, then we label B as `on`.

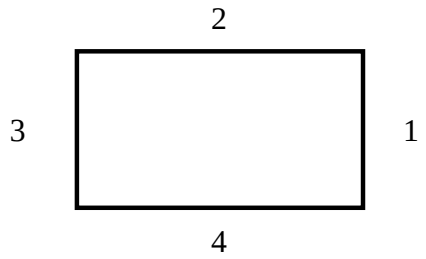

Figure 3: The labelling of boxes intersecting an oval.

The third, and most complicated, part of our program is the change of variables in the boxes that intersect the oval. Let $b \in B$ be the midpoint of B. Compute

$$u = \nabla H(b),$$

and choose v such that

$$u \perp v \quad \text{and} \quad v_1 \geq 0.$$

Using the labelling illustrated in Figure 3, let `right` and `left` be the sides intersected by the line $b + tv$, $t \in \mathbb{R}$. Denote the intersection points by p, and q, respectively. The possible configurations of an intersection of the oval with a box are illustrated in Figure 4. The restriction of H to the sides `right` and `left`, respectively, are one-dimensional functions, and the location of the intersections can be approximated, and their uniqueness proved, using the interval Newton method [23] initialised from the points p, and q, respectively. Let,

$$\texttt{accuracy} = \texttt{minsize}/10.$$

Define the points p_{up}, p_{down} on the `right`-side and the points q_{up}, q_{down} on the `left`-side at the distance `accuracy` from p and q, respectively, as illustrated in Figure 5.

If the following conditions hold, then the oval is inside the tube illustrated in Figure 5, and we can change coordinates to get a small box, which is guaranteed to contain the segment of the oval passing through B. This small box represents the error caused by the unknown location of the oval.

Condition 5.1.

$$\begin{aligned} \text{sign}\,(H(p_{up}) - h) &= \text{sign}(H(q_{up}) - h) \\ &= -\text{sign}(H(p_{down}) - h) \\ &= -\text{sign}(H(q_{down}) - h) \end{aligned} .$$

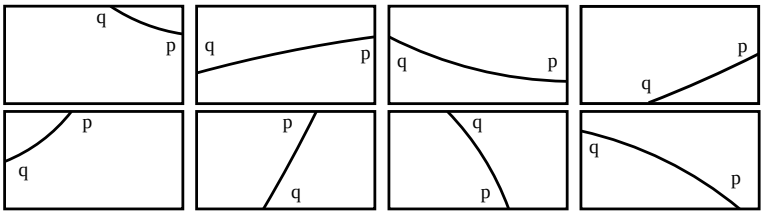

Figure 4: The possible configurations of the intersection of an oval and a box.

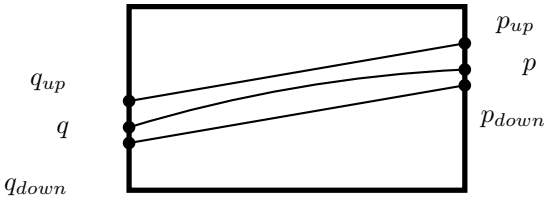

Figure 5: Constructing a small, local enclosure of the oval.

Let l_{up}, and l_{down} denote the line segments between p_{up} and q_{up}, and p_{down} and q_{down}, respectively. Denote by H' differentiation with respect to the parametrisation of the line l_{up}, and l_{down}, respectively.

Condition 5.2.

$$0 \notin (H(l_{up}) - h) \quad \text{or} \quad 0 \notin H'(l_{up})$$
$$0 \notin (H(l_{down}) - h) \quad \text{or} \quad 0 \notin H'(l_{down}).$$

Let `otherside1`, and `otherside2` be the two other sides of the box B, that is,

$$\texttt{otherside1} \cup \texttt{otherside2} \cup \texttt{right} \cup \texttt{left} = \{1, 2, 3, 4\}.$$

Condition 5.3.

$$\Gamma_h \cap \texttt{otherside1} = \emptyset \quad \text{and} \quad \Gamma_h \cap \texttt{otherside2} = \emptyset,$$

We enclose the segment of the oval inside of the box between two straight lines: Condition 5.1 guarantees that the points p_{up}, p_{down}, q_{up}, and q_{down} are on different sides of the oval as in Figure 5, Condition 5.2 guarantees that the lines l_{up} and l_{down} do not intersect the oval, and Condition 5.3 guarantees that the oval does not cross the other sides of the box. Recall that the uniqueness of p and q is proved as they are approximated. Hence, we have proved that the segment of the oval crossing the box has exactly two intersections with the boundary of the box, and that it is confined to the region between l_{up} and l_{down}.

If (5.1), (5.2), and (5.3), hold, then we set `accuracy=accuracy/2`, re-calculate p_{up}, p_{down}, q_{up}, and q_{down}, and try to verify (5.1), (5.2), and (5.3). This procedure is iterated until (5.1), or (5.2) do not hold. Finally, we label B as `on`.

The fourth and final part of our integration algorithm, is the actual integration. The integration is done separately for the boxes that are labelled, `inside`, `fail`, and `on`.

If B is `inside` we compute

$$\int_B x^i y^j \, dx \wedge dy = \left(\frac{\sup(B_1)^{i+1}}{i+1} - \frac{\inf(B_1)^{i+1}}{i+1} \right) \left(\frac{\sup(B_2)^{j+1}}{j+1} - \frac{\inf(B_2)^{j+1}}{j+1} \right). \tag{16}$$

If B is labelled `fail`, we know that B might intersect the oval, that is, we have neither been able to prove intersection, nor non-intersection. Therefore, we must include any possible result; the integral over B is calculated as the interval hull of 0 and the largest, and smallest, respectively, result of (16) calculated on a subbox $\tilde{B} \subset B$.

Boxes labelled `fail` cause large over-estimations. Fortunately such boxes are rare, typically less than 5% of the `on`-boxes, see Section 6. If `minsize` is taken sufficiently small, the effect of the `fail`-boxes is negligible.

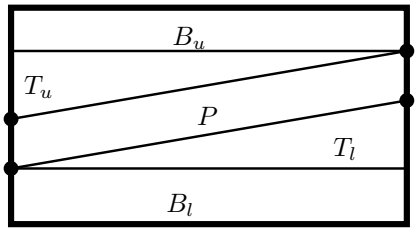

Figure 6: The change of variables splitting.

The boxes that are labelled `on`, are split into five parts, as illustrated in Figure 6. By construction, none of the triangles, T_l, T_u, or boxes B_l, B_u in the splitting of B intersect the oval, thus it suffices to evaluate H in one point of each, and hence they can all be labelled as `inside` or `outside`. The boxes B_l, B_u are then treated as above, that is, if they are labelled `inside` they are integrated according to (16), and if they are labelled `outside` they are neglected. A triangle labelled `outside` is also neglected, the integrals on triangles labelled `inside` are enclosed by the formula

$$\int_T x^i y^j \, dx \wedge dy \in \Box T_1^i \Box T_2^j |T|, \tag{17}$$

where $\Box T$ is the box hull of T, and $|T|$ is the area of T. This gives a reasonably narrow enclosure of the integral, since the width of $\Box T$ is typically small. The parallelepiped, P, which covers the segment of the oval, remains to be studied. When we integrate over P, the same problem as in the `fail` case occurs; we do not know how much of the parallelepiped to include. Therefore, we have to take the hull of all possible outcomes. Hence, the integrals are computed as

$$\int_P x^i y^j \, dx \wedge dy \in \text{Hull}\left(0, \Box P_1^i \Box P_2^j |P|\right), \tag{18}$$

where $\Box P$ is the box hull of P and $|P|$ is the area of P.

The value of the Abelian integral is enclosed by summing over all the computed integrals that are labelled as either `inside`, `fail`, or `on`.

$$\begin{array}{rcl} I(h) & \in & \sum_{B \in \texttt{inside}} (16) + \sum_{T \in \texttt{inside}} (17) \\ & + & \sum_{B \in \texttt{fail}} \text{Hull}(0, (16)) \\ & + & \sum_{P \in \texttt{on}} (18) \end{array} \tag{19}$$

6 Computational results

In this section we apply the methods developed in Section 5.3 to the elliptical Hamiltonians of degree four, described in Section 2. The main idea we use in all examples is to integrate monomial forms at some points, and then to specify the coefficients of ω such that $I(h)$ is zero at the sampled points. Therefore, let

$$I_{ij}(h) = \int_{D_h} x^i y^j \, dx \wedge dy. \tag{20}$$

For the cases (i), (ii), (iv), where we give examples of perturbations yielding bifurcations with less limit cycles than coefficients, we sample at the corresponding number of h-values, uniformly distributed between the saddle loops and the singularity. Together with a normalisation of one of the coefficients, this procedure gives a linear system of equations, from which candidate coefficients can be deduced.

Given some candidate coefficients of the form ω, we calculate the $I_{ij}(h)$, at intermediate ovals. If the linear combination of the $I_{ij}(h)$ has validated sign changes between the sample points we are done: it has been proved that the corresponding perturbation yields bifurcations with the given number of limit cycles as $\epsilon \to 0$.

All computations were performed on a Intel Xeon 2.0 Ghz, 64bit processor with 7970Mb of RAM. The program was compiled with `gcc`, version 3.4.6. The software for interval arithmetic was provided by the `CXS-C` package, version 2.1.1, see [4, 18].

6.1 The truncated pendulum

The Hamiltonian with a phase portrait called the truncated pendulum, see Figure 1(i), is given by, see [6],

$$H = \frac{y^2}{2} - \frac{x^4}{4} + \frac{x^2}{2}. \tag{21}$$

The corresponding differential system has one centre and two saddles; the saddles are connected by two heteroclinic orbits at $H = \frac{1}{4}$.

We compute the values of $I_{ij}(h_k)$ for $(i,j) \in \{(0,0),(2,0),(0,2)\}$, and $h_k = k\frac{1}{24}$, where $k = 1, ..., 5$; the coefficient in front of I_{10} is assumed to be zero. The values are shown in Table 1.

h_k	I_{00}	I_{20}	I_{02}
$\frac{1}{24}$	[0.2649,0.2672]	[0.005695,0.005845]	[0.005433,0.005601]
$\frac{2}{24}$	[0.5405,0.5437]	[0.02433,0.02475]	[0.02215,0.02253]
$\frac{3}{24}$	[0.8287,0.8327]	[0.05894,0.05990]	[0.05052,0.05126]
$\frac{4}{24}$	[1.135,1.140]	[0.1150,0.1166]	[0.09139,0.09248]
$\frac{5}{24}$	[1.470,1.475]	[0.2035,0.2057]	[0.1454,0.1468]

Table 1: The computed enclosures for the truncated pendulum.

We put $\delta = 1$, and solve the linear system for the coefficients α, and γ, so that

$$\alpha \check{I}_{00}^{h_k} + \gamma \check{I}_{20}^{h_k} + \check{I}_{02}^{h_k} = 0, \quad k = 2, 4\,, \tag{22}$$

where $\check{I}_{ij}^{h_k}$ denotes the midpoint of $I_{ij}(h_k)$. The approximate solution that we use as our perturbation is $\alpha = -0.009510238485402$, and $\gamma = -0.700351938113869$.

To prove that the perturbed system has two limit cycles at $H = \frac{1}{12}$, and $H = \frac{2}{12}$, respectively, we compute $I(h)$, at the intermediate ovals,

$$\begin{array}{rcl} I(\frac{1}{24}) & = & [-0.001191, -0.0009075], \\ I(\frac{3}{24}) & = & [+0.0006606, +0.002093], \\ I(\frac{5}{24}) & = & [-0.01257, -0.009753]. \end{array} \tag{23}$$

Hence, the system with the given perturbation has two limit cycles, one attracting from approximately $H = \frac{2}{12}$, and one repelling from approximately $H = \frac{1}{12}$, see Figure 2(i). The run-time of the program was 33 seconds, a total of 648 boxes were used to cover the 5 ovals, 76 of these belong to the `fail` class.

6.2 The Saddle loop

The Hamiltonian with a phase portrait called the saddle loop, see Figure 1(ii), is given by, see [6],

$$H = \frac{y^2}{2} - \frac{x^4}{4} - \frac{\lambda - 1}{3}x^3 + \frac{\lambda}{2}x^2, \tag{24}$$

where $\lambda \in (1, \infty)$. The corresponding differential system has one centre surrounded by a homoclinic orbit. We study $\lambda = 4$, to give an example and display what our method can do; another choice of λ should give similar results. For this Hamiltonian, the homoclinic orbit is located at $H = \frac{3}{4}$.

We compute the values of $I_{ij}(h)$ for $(i, j) \in \{(0,0), (1,0), (2,0), (0,2)\}$, for $h_k = k\frac{3}{32}$, where $k = 1, ..., 7$. The values are shown in Table 2.

h_k	I_{00}	I_{10}	I_{20}	I_{02}
$\frac{3}{32}$	[0.2968,0.2969]	[0.002706,0.002707]	[0.003572,0.003573]	[0.01387,0.01388]
$\frac{6}{32}$	[0.5990,0.5991]	[0.01136,0.01137]	[0.01484,0.01485]	[0.05583,0.05584]
$\frac{9}{32}$	[0.9073,0.9074]	[0.02700,0.02701]	[0.03486,0.03487]	[0.1263,0.1264]
$\frac{12}{32}$	[1.223,1.224]	[0.05106,0.05107]	[0.06509,0.06511]	[0.2261,0.2262]
$\frac{15}{32}$	[1.548,1.549]	[0.08569,0.08570]	[0.1077,0.1078]	[0.3560,0.3561]
$\frac{18}{32}$	[1.887,1.888]	[0.1345,0.1346]	[0.1665,0.1666]	[0.5169,0.5167]
$\frac{21}{32}$	[2.246,2.247]	[0.2054,0.2055]	[0.2492,0.2493]	[0.7105,0.7106]

Table 2: The computed enclosures for the saddle loop.

We put $\gamma = 1$, and solve the linear system for the coefficients α, β, and δ, so that

$$\alpha\check{I}_{00}^{h_k} + \beta\check{I}_{10}^{h_k} + \check{I}_{20}^{h_k} + \delta\check{I}_{02}^{h_k} = 0, \quad k = 2, 4, 6\,. \tag{25}$$

The approximate solution we use as our perturbation is $\alpha = -0.000010932964822$, $\beta = -0.991766031106913$, and $\delta = -0.063860197399010$.

To prove that the perturbed system has three limit cycles bifurcating from $H = \frac{3}{16}$, $H = \frac{6}{16}$, and $H = \frac{9}{16}$, respectively, we compute $I(h)$ at the intermediate ovals:

$$\begin{array}{rcl} I(\frac{3}{32}) & = & [-0.000001405, -0.0000009097], \\ I(\frac{9}{32}) & = & [+0.0000001299, +0.000001812], \\ I(\frac{15}{32}) & = & [-0.000004034, -0.0000009977], \\ I(\frac{21}{32}) & = & [+0.00003338, +0.00003793]. \end{array} \tag{26}$$

Hence, the system with the given perturbation has three limit cycles, one attracting from approximately $H = \frac{6}{16}$, and two repelling from approximately $H = \frac{3}{16}$, and $H = \frac{9}{16}$, respectively, see Figure 2(ii). The run-time of the program was 94 minutes and 33 seconds, a total of 85916 boxes were used to cover the 7 ovals, 3944 of these belong to the `fail` class.

6.3 The Cuspidal loop

The Hamiltonian with a phase portrait called the cuspidal loop, see Figure 1(iv), is given by, see [7],

$$H = \frac{y^2}{2} + \frac{x^4}{4} + \frac{1}{3}x^3, \tag{27}$$

The corresponding differential system has one centre at $H = -\frac{1}{12}$ surrounded by a cuspidal loop, located at $H = 0$.

We compute the values of $I_{ij}(h)$ for $(i,j) \in \{(0,0),(1,0),(2,0),(0,2)\}$, for $h_k = -k\frac{1}{96}$, where $k = 1, ..., 7$. The values are shown in Table 3.

h_k	I_{00}	I_{10}	I_{20}	I_{02}
$-\frac{1}{96}$	[0.5344,0.5345]	[-0.4739,-0.4738]	[0.4496,0.4497]	$[1.823,1.824]10^{-2}$
$-\frac{2}{96}$	[0.4414,0.4414]	[-0.4030,-0.4029]	[0.3867,0.3868]	$[1.315,1.316]10^{-4}$
$-\frac{3}{96}$	[0.3577,0.3578]	[-0.3339,-0.3338]	[0.3232,0.3233]	$[9.003,9.004]10^{-3}$
$-\frac{4}{96}$	[0.2797,0.2798]	[-0.2658,-0.2657]	[0.2593,0.2594]	$[5.687,5.688]10^{-3}$
$-\frac{5}{96}$	[0.2057,0.2058]	[-0.1985,-0.1984]	[0.1949,0.1950]	$[3.161,3.162]10^{-3}$
$-\frac{6}{96}$	[0.1348,0.1349]	[-0.1318,-0.1317]	[0.1303,0.1304]	$[1.389,1.391]10^{-3}$
$-\frac{7}{96}$	[0.06637,0.06638]	[-0.06566,-0.06565]	[0.06530,0.06531]	$[3.440,3.441]10^{-4}$

Table 3: The computed enclosures for the cuspidal loop.

We put $\gamma = 1$, and solve the linear system for the coefficients α, β, and δ, so that

$$\alpha \check{I}_{00}^{h_k} + \beta \check{I}_{10}^{h_k} + \check{I}_{20}^{h_k} + \delta \check{I}_{02}^{h_k} = 0, \quad k = 2, 4, 6\,. \tag{28}$$

The approximate solution that we use as our perturbation is $\alpha = 0.233937272601683$, $\beta = 1.234119595803674$, and $\delta = 0.559050361812264$.

To prove that the perturbed system has three limit cycles bifurcating from $H = -\frac{1}{48}$, $H = -\frac{2}{48}$, and $H = -\frac{3}{48}$, respectively, we compute $I(h)$, at the intermediate ovals,

$$\begin{array}{rcl} I(-\frac{1}{96}) & = & [+0.0001742, +0.00001815], \\ I(-\frac{3}{96}) & = & [-0.00001366, -0.000007643], \\ I(-\frac{5}{96}) & = & [+0.000001450, +0.000006194], \\ I(-\frac{7}{96}) & = & [-0.000005781, -0.000002956]. \end{array} \tag{29}$$

Hence, the system with the given perturbation has three limit cycles: one attracting from approximately $H = -\frac{2}{48}$, and two repelling from approximately $H = -\frac{1}{48}$, and $H = -\frac{3}{48}$, respectively, see Figure 2(iii). The run-time of the program was 54 minutes and 13 seconds, a total of 55898 boxes were used to cover the 7 ovals, 2566 of these belong to the `fail` class.

6.4 The Figure eight loop

The Hamiltonian with a phase portrait called the figure eight loop, see Figure 1(v), is given by,

$$H = \frac{y^2}{2} + \frac{x^4}{4} + \frac{1-\lambda}{3}x^3 - \frac{\lambda}{2}x^2, \tag{30}$$

where $\lambda \in (0,1)$, see [9]. The corresponding differential system has two centres, at $H = -\frac{1}{12}(2\lambda+1)$, and $H = -\frac{1}{12}\lambda^3(\lambda+2)$, that are surrounded by a figure eight loop, located at $H = 0$. As λ grows the right loop grows; $\lambda = 1$ is a symmetric figure eight loop. We choose to study $\lambda = 0.95$; a motivation why we want λ large is given below.

In [29] Petrov proves that when restricting to one family of ovals, surrounding one of the two centres, the space of Abelian integrals has dimension 4, and that the space has the Chebyshev property, that is, the number of zeros of a function in this space is less than the dimension of the space. He also proves that this bound is sharp. To construct an example with more than three limit cycles surrounding either of the two centres, we can therefore not use the previous method.

Our heuristic argument to guess parameters is the following: we start by integrating at 100 uniformly distributed ovals, in each eye of the loop. We do this with moderate accuracy, which gives a fast and sufficiently precise result. Since we have chosen to study a figure eight loop that is not far from being symmetric, it is reasonable to assume that the two branches behave similarly, which makes it probable that we should be able to determine coefficients so that each branch has two zeros. To determine such zeros, we solve the following linear system:

$$\begin{bmatrix} I_{00}^l(-0.0362) & I_{10}^l(-0.0362) & I_{20}^l(-0.0362) & I_{02}^l(-0.0362) \\ I_{00}^l(-0.1208) & I_{10}^l(-0.1208) & I_{20}^l(-0.1208) & I_{02}^l(-0.1208) \\ I_{00}^l(-0.1812) & I_{10}^l(-0.1812) & I_{20}^l(-0.1812) & I_{02}^l(-0.1812) \\ I_{00}^r(-0.1054) & I_{10}^r(-0.1054) & I_{20}^r(-0.1054) & I_{02}^r(-0.1054) \end{bmatrix} \begin{bmatrix} \alpha \\ \beta \\ \gamma \\ \delta \end{bmatrix} = \begin{bmatrix} 1 \\ -1 \\ 1 \\ -1 \end{bmatrix} \tag{31}$$

where $I_{ij}^l(h)$, and $I_{ij}^r(h)$, denote the monomial Abelian integrals calculated on the left and right ovals, respectively.

This gives the approximate solution $\alpha = 438.4905$, $\beta = -25.2469$, $\gamma = -452.7899$, and $\delta = -741.0341$, which we use as our perturbation. The graph of the resulting function is given in Figure 7, which appears to have 4 zeros. This, of course, has to be proved.

To prove that the perturbation constructed above has 4 zeros, we procede as in the previous examples, and compute enclosures of the Abelian integral at intermediate ovals. On the left branch we calculate $I(-0.0121)$, $I(-0.0846)$, and $I(-0.1933)$, and on the right branch we compute $I(-0.0105)$, $I(-0.0738)$, and $I(-0.1686)$. The result is given in Tables 4, and 5.

Finally, we compute $I^l(h)$, and $I^r(h)$ at the intermediate ovals,

$$\begin{array}{rcl} I^l(-0.0121) & = & [+8.698, +9.290], \\ I^l(-0.0846) & = & [-2.204, -1.780], \\ I^l(-0.1933) & = & [+0.9121, +1.119], \\ I^r(-0.0105) & = & [+11.56, +12.10], \\ I^r(-0.0738) & = & [-1.181, -0.7959], \\ I^r(-0.1686) & = & [+0.2095, +0.3847] \end{array} . \tag{32}$$

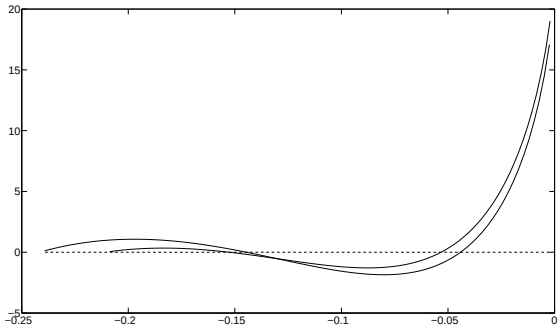

Figure 7: The two branches of the Abelian Integral for the figure eight loop.

h	I^l_{00}	I^l_{10}	I^l_{20}	I^l_{02}
-0.0121	[1.206,1.207]	[-1.034,-1.033]	[0.9945,0.9951]	[0.1290,0.1293]
-0.0846	[0.7661,0.7665]	[-0.7073,-0.7068]	[0.6902,0.6907]	[0.05829,0.05839]
-0.1933	[0.2219,0.2222]	[-0.2178,-0.2175]	[0.2160,0.2164]	[0.005326,0.005340]

Table 4: The computed enclosures for the left branch of the figure eight loop.

h	I^r_{00}	I^r_{10}	I^r_{20}	I^r_{02}
-0.0105	[1.077,1.078]	[0.8773,0.8778]	[0.8033,0.8039]	[0.1006,0.1008]
-0.0738	[0.6846,0.6851]	[0.6002,0.6006]	[0.5573,0.5577]	[0.04545,0.04553]
-0.1686	[0.1984,0.1987]	[0.1848,0.1850]	[0.1744,0.1747]	[0.004154,0.004164]

Table 5: The computed enclosures for the right branch of the figure eight loop.

Hence, the system with the given perturbation has four limit cycles, one attracting and one repelling inside each loop, see Figures 2(iv) and 8. The run-time of the program was, for the left (right) branch, 82 (78) seconds, a total of 1182 (1166) boxes were used to cover the 3 ovals, 82 (56) of these belong to the `fail` class.

To prove that the unstable separatrices of the saddle are attracted to a limit cycle enclosing the figure eight loop, as indicated in Figure 8, we first calculate $I^o(h)$, the outer Abelian integral, for some $h > 0$ values with low accuracy to find an indication of a sign change. It appears that a limit cycle bifurcates from an oval close to $H = 0.1$. Therefore, we compute $I^o(0.09)$, and $I^o(0.11)$,

$$\begin{aligned} I^o(0.09) &= [+8.715, +24.83], \\ I^o(0.11) &= [-25.37, -9.821]. \end{aligned} \tag{33}$$

These calculations verify that the perturbed system has an attracting limit

h	I^o_{00}	I^o_{10}	I^o_{20}	I^o_{02}
0.09	[3.576,3.587]	[-0.1843,-0.1709]	[2.560,2.575]	[0.5307,0.5376]
0.11	[3.776,3.786]	[-0.1862,-0.1740]	[2.708,2.724]	[0.6044,0.6109]

Table 6: The computed enclosures for the outside of the figure eight loop.

cycle bifurcating from an oval outside the figure eight loop. The run-time of the program was 39 seconds, a total of 496 boxes were used to cover the 2 ovals, 52 of these belong to the `fail` class.

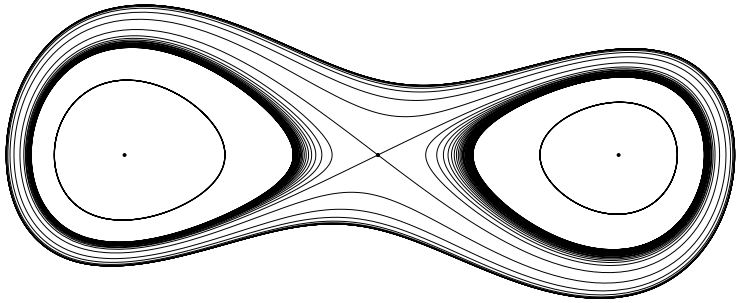

Figure 8: The perturbed figure eight loop, with $\epsilon = 0.001$.

7 Conclusions

We have presented a method to rigorously calculate Abelian integrals. The method can be applied to study any polynomial perturbation of a polynomial Hamiltonian vector field. We have applied the method to the case of elliptic Hamiltonians of degree 4, and given some indications of what happens in the case of a general perturbation, compared to the Liénard case, studied by Dumortier and Li in [6, 7, 8, 9].

The method can be used in several ways: either one can use it to verify that a specific perturbation guessed by some other method indeed has a certain number of zeros, or one can use it as in Section 6.4 to sample and plot the monomial Abelian integrals. In the latter case, if a good choice of parameters can be made from the approximate knowledge of the monomial Abelian integrals, then one can re-use the program to verify that guess, as is done in Section 6.4.

A major challenge is to device a method which can be used to guess what perturbations to investigate. One such method that appears in the literature is that of a detection function, as used in e.g. [33]. Another problem, which we have ignored in this paper, is that typically when one has a Hamiltonian depending on parameters, the maximal number of limit cycles that can bifurcate from one member of this family, will only appear for some special values of the parameters. It would therefore be desirable to develop conditions indicating how to choose one candidate system from a family. In Section 6.4 we give a completely heuristic argument why we want to have λ large.

7.1 Future work

We intend to apply the presented method to hyperelliptic Hamiltonians, for which few results have been proved; the most important is the result by Novikov and Yakovenko [26], which states that the number of limit cycles that can bifurcate from a hyperelliptic Hamiltonian is bounded by a certain tower function. Results on the exact number of zeros in some special cases can be found in [13].

The most important further development of the algorithm is to find a sound way to select perturbations, when the space of Abelian integrals does not have the Chebyshev property.

References

[1] G. Alefeld, and J. Herzberger, Introduction to Interval Computations, Academic Press, New York, 1983.

[2] F. Chen, C. Li, J. Llibre, Z. Zhang, A unified proof on the weak Hilbert 16th problem for $n = 2$. J. Differential Equations 221 (2006), no. 2, 309–342.

[3] C. Christopher, C. Li, Limit cycles of differential equations. Advanced Courses in Mathematics. CRM Barcelona. Birkhäuser Verlag, Basel, 2007.

[4] CXSC – C++ eXtension for Scientific Computation, version 2.0. Available from http://www.math.uni-wuppertal.de/org/WRST/xsc/cxsc.html

[5] G. F. D. Duff, Limit-cycles and rotated vector fields. Ann. of Math. (2) 57, (1953). 15–31

[6] F. Dumortier, C. Li, Perturbations from an elliptic Hamiltonian of degree four. I. Saddle loop and two saddle cycle. J. Differential Equations 176 (2001), no. 1, 114–157.

[7] F. Dumortier, C. Li, Perturbations from an elliptic Hamiltonian of degree four. II. Cuspidal loop. J. Differential Equations 175 (2001), no. 2, 209–243.

[8] F. Dumortier, C. Li, Perturbation from an elliptic Hamiltonian of degree four. III. Global centre. J. Differential Equations 188 (2003), no. 2, 473–511.

[9] F. Dumortier, C. Li, Perturbation from an elliptic Hamiltonian of degree four. IV. Figure eight-loop. J. Differential Equations 188 (2003), no. 2, 512–554.

[10] F. Dumortier, R. Roussarie, Abelian integrals and limit cycles. J. Differential Equations 227 (2006), no. 1, 116–165.

[11] Écalle, Jean Introduction aux fonctions analysables et preuve constructive de la conjecture de Dulac. (French) [Introduction to analyzable functions and constructive proof of the Dulac conjecture] Actualités Mathématiques. [Current Mathematical Topics] Hermann, Paris, 1992.

[12] D. Gabai, G. R. Meyerhoff, N. Thurston, Homotopy hyperbolic 3–manifolds are hyperbolic. Ann. of Math. (2) 157 (2003), no. 2, 335–431.

[13] L. Gavrilov, I.D. Iliev, Complete hyperelliptic integrals of the first kind and their non-oscillation. Trans. Amer. Math. Soc. 356 (2004), no. 3, 1185–1207.

[14] J. Guckenheimer, P. Holmes, Nonlinear Oscillations, Dynamical Systems, and Bifurcations of Vector Fields, Applied Mathematical Sciences, 42. Springer-Verlag, New York, 1983.

[15] J. Guckenheimer, Phase portraits of planar vector fields: computer proofs. Experiment. Math. 4 (1995), no. 2, 153–165.

[16] J. Guckenheimer, S. Malo, Computer-generated proofs of phase portraits for planar systems. Internat. J. Bifur. Chaos Appl. Sci. Engrg. 6 (1996), no. 5, 889–892.

[17] T. C. Hales, A proof of the Kepler conjecture. Ann. of Math. (2) 162 (2005), no. 3, 1065–1185.

[18] R. Hammer, M. Hocks, U. Kulisch, and D. Ratz, C++ Toolbox for Verified Computing, Springer-Verlag, New York, 1995.

[19] Yu. S. Il'yashenko, Finiteness theorems for limit cycles. Translated from the Russian by H. H. McFaden. Translations of Mathematical Monographs, 94. American Mathematical Society, Providence, RI, 1991.

[20] Yu. S. Il'yashenko, Centennial history of Hilbert's 16th problem. Bull. Amer. Math. Soc. (N.S.) 39 (2002), no. 3, 301–354

[21] C. Liu, Estimate of the number of zeros of Abelian integrals for an elliptic Hamiltonian with figure-of-eight loop. Nonlinearity 16 (2003), no. 3, 1151–1163.

[22] S. Malo, Rigorous Computer Verification of Planar Vector Field Structure, Ph.D thesis, Cornell University, 1994.

[23] R.E. Moore, Interval Analysis, Prentice-Hall, Englewood Cliffs, New Jersey, 1966.

[24] R.E. Moore, Methods and Applications of Interval Analysis, SIAM Studies in Applied Mathematics, Philadelphia, 1979.

[25] A. Neumaier, Interval Methods for Systems of Equations. Encyclopedia of Mathematics and its Applications 37, Cambridge Univ. Press, Cambridge, 1990

[26] D. Novikov, S. Yakovenko, Tangential Hilbert problem for perturbations of hyperelliptic Hamiltonian systems. Electron. Res. Announc. Amer. Math. Soc. 5 (1999), 55–65

[27] M.S. Petković, L.D. Petković, Complex interval arithmetic and its applications. Mathematical Research, 105. Wiley-VCH Verlag Berlin GmbH, Berlin, 1998.

[28] G.S. Petrov, Elliptic integrals and their nonoscillation. (Russian) Funktsional. Anal. i Prilozhen. 20 (1986), no. 1, 46–49, 96.

[29] G.S. Petrov, Nonoscillation of elliptic integrals. (Russian) Funktsional. Anal. i Prilozhen. 24 (1990), no. 3, 45–50, 96; translation in Funct. Anal. Appl. 24 (1990), no. 3, 205–210 (1991)

[30] G.S. Petrov, On the nonoscillation of elliptic integrals. (Russian) Funktsional. Anal. i Prilozhen. 31 (1997), no. 4, 47–51, 95; translation in Funct. Anal. Appl. 31 (1997), no. 4, 262–265 (1998)

[31] R. Roussarie, Bifurcation of planar vector fields and Hilbert's sixteenth problem. Progress in Mathematics, 164. Birkhäuser Verlag, Basel, 1998.

[32] W. Tucker, A rigorous ODE solver and Smale's 14th problem. Found. Comput. Math. 2 (2002), no. 1, 53–117.

[33] H. Zhou,W. Xu, S. Li, Y. Zhang, On the number of limit cycles of a cubic polynomials Hamiltonian system under quintic perturbation. (English summary) Appl. Math. Comput. 190 (2007), no. 1, 490–499.